ASEC 2022

MDPI

Proceedings

Additive effects of lanthanide compound into $CH_3NH_3PbI_3$ perovskite layer on the photovoltaic properties and electronic structure

Atsushi Suzuki[1]*, Kyo Kishimoto[1], Takeo Oku[1], Masanobu Okita[2], Sakiko Fukunishi[2], Tomoharu Tachikawa[2], and Tomoya Hasegawa [2]

[1] Department of Materials Science, The University of Shiga Prefecture, Japan; ov21kkishimoto@ec.usp.ac.jp, oku@mat.usp.ac.jp
[2] Osaka Gas Chemicals Co., Ltd., Japan; okita@ogc.co.jp, fukunishi@ogc.co.jp, t-tachikawa@ogc.co.jp; hasegawa_tomoya@ogc.co.jp
* Correspondence: suzuki@mat.usp.ac.jp; Tel.: +81-749-28-8369 (A. S.)

Abstract: Lanthanide compound doped $CH_3NH_3PbI_3$ ($MAPbI_3$) perovskite solar cells have been fabricated and characterized. The purpose of this research is to investigate additive effect of formamidinium iodine (FAI) and lanthanide compound into the $MAPbI_3$ perovskite layer for improving the photovoltaic performance and the stability of conversion efficiency. Incorporation of FAI and europium chloride into the perovskite crystals maintained the stability of conversion efficiency for 30 days. The photovoltaic performance was based on the narrow band dispersion with decrease of effective mass related to the carrier mobility. The carrier mobility depends on the degree of charge transfer between 3d orbital of europium atom, 5p orbital of iodine atom and 6p orbital of lead atom in the perovskite crystal. Addition of samarium or terbium compound into the crystal reduced the photovoltaic performance due to the flat band dispersion of d orbital of samarium atom or 4f orbital of terbium atom near valence band state. The lanthanide-doped perovskite crystal controlled the photovoltaic characteristics based on the electronic structure. The europium-doped perovskite crystal have advantage to apply for the industrial photovoltaic devices with stability.

Keywords: perovskite solar cells; lanthanide compound; photovoltaic properties; morphology; X-ray diffraction; first-principles calculation

Citation: Lastname, F.; Lastname, F.; Lastname, F. Title. *Appl. Sci.* **2022**, *12*, x. https://doi.org/10.3390/xxxxx

Academic Editor: Firstname Lastname

Received: date
Accepted: date
Published: date

1. Introduction

The perovskite solar cells have great performances of photovoltaic properties, as compared with characteristics of silicon and gallium arsenide solar cells [1, 2]. The perovskite solar cell have these issues concerning the photovoltaic performance related to stability. The perovskite solar cells were composed of the perovskite layer as active layer, electron and hole-transporting layer. Material design of the perovskite crystal is important to develop the photovoltaic device with stability of the photovoltaic performance. For example, the $CH_3NH_3PbX_3$ ($MAPbX_3$) perovskite crystal with substitution of alkali metal ions such as sodium, potassium, rubidium and cesium [3-8], organic cation [9,10] such as formamidinium (FA), guanidinium (GA), ethylammonium (EA) [11] as A-site, tin [12], transition metal [13-16], lanthanides using europium (Eu) [17, 18], samarium (Sm), and terbium (Tb) ion as B-site and halogen ions as X-site have been characterized [19-23].

Recently, partial substitution of lead (Pb)-site by lanthanide ion such as Eu^{3+}, cerium (Ce^{3+}), or neodymium ions passivated the interface morphology while suppressing the decomposition by Eu^{2+}/Eu^{3+} redox reaction [24-26]. The photovoltaic properties depended

on interface, internal morphology, the band structure near valence and conduction band states, thermodynamics and kinetic behavior. The band dispersion and effective mass has been studied for expecting the carrier diffusion and mobility related to short-circuit current density, and conversion efficiency. The lanthanide compounds with luminescence characteristics have been applied as up/down conversion materials for solar cells [27, 28].

Our purpose is to fabricate and characterize the lanthanide compounds-doped $MAPbX_3$ perovskite solar cells for improving the photovoltaic performance and conversion efficiency. Especially the photovoltaic characteristics of the perovskite solar cell added with europium hydride compounds, samarium or terbium acetylacetonate hydrate was investigated. The photovoltaic properties were analyzed by the *J-V* characteristics, morphology and electronic structure.

2. Materials and Methods

The lanthanide compound-doped $MAPbI_3$ perovskite solar cells using decaphenylcyclopentasilane (DPPS) were fabricated and characterized [29, 30]. The photovoltaic cells were fabricated as FTO/TiO_2/perovskite/DPPS/Spiro-OMeTAD/Au. The *J–V* characteristics (Keysight B2901A, Keysight Technologies, Santa Rosa, CA, USA) were measured under illumination at 100 mW cm^{-2} by using an AM 1.5 solar simulator (San-ei Electric XES-301S, Osaka, Japan). The solar cells were illuminated through the side of the FTO substrates and the measurement area was 0.080 cm^2. The photovoltaic parameters, open circuit voltage (V_{oc}), short circuit current density (J_{sc}), fill factor (*FF*), series resistance (R_s), shunt resistance (R_{sh}) and conversion efficiency (η) were measured. The external quantum efficiency (EQE, QE-R, Enli Technology Co. Ltd., Kaohsiung, Taiwan) was measured.

The Eu^{3+}, Sm^{2+}, Sm^{2+} or Tb^{3+}-doped $FAPbI_3$ and $FAPbI_3$ perovskite crystal were formed as a cubic crystal using experimental lattice constants ($FAPbI_3$: a = 6.3621 Å) measured by X-ray diffraction data [31-33]. The $FAPbI_3$ perovskite crystals (cubic *Pm*3*m*) were constructed with supercells (2×2×2). The mole ratio of the Eu^{3+}, Eu^{2+}, Sm^{2+} or Tb^{3+} ions to Pb^{2+} cation ion was adjusted to be 1:8 as 12.5 %. The ab initio quantum calculations were performed using the Vanderbilt ultrasoft pseudo-potentials, scalar relativistic generalized gradient approximations and Perdew-Burke-Ernzerhof (GGA-PBE) exchange-correlation functional and density functional theory (DFT+U, U = 6.0 eV) (Quantum Espresso, v.5.2.1, Quantum Espresso Foundation, UK). Plane-wave basis set cut offs for the wave functions and charge density were used to be 30 and 320 Rydberg (Ry). Uniform *k*-point grid (4×4×4) or (8×8×8) in the Brillouin zone was used.

The Eu^{2+} or Sm^{2+}-doped $FAPbI_3$ perovskite crystal was fixed to be neutral state in the unit cell. The Tb^{3+}-doped $FAPbI_3$ perovskite crystal was fixed to be +1 charge state in the unit cell. The band structures were analyzed for the Brillouin zone along the direction of wave vector. Path for the Eu^{2+}, Sm^{2+} or Tb^{3+}- doped $FAPbI_3$ perovskite crystals were set as follows, Γ (0, 0, 0)→X (0, ½, 0)→M (1/2, 1/2, 0)→Γ→R (1/2, 1/2, 1/2)→X, M→R. Pb cation was set at the position of Γ (0, 0, 0). The energy levels were standardized with Fermi energy at zero. The partial density of state (PDOS) near valence (VB) and conduction (CB) band states were calculated.

3. Results and Discussion

The *J-V* characteristics and EQE of the perovskite solar cell doped with FAI and lanthanide compounds were investigated. The photovoltaic parameters of J_{SC}, *FF*, *R*s, R_{sh} and EQE of the perovskite solar cell added with 10% FAI and 2% $EuCl_2$ were improved, yielding the best value of η to be 9.94%. In the cases of 20% FAI and 2 % $EuCl_2$ or 20% FAI, the *J-V* curves exhibited the hysteresis behavior during the scanning direction. This behavior was due to no-uniformity of carrier diffusion through the grains boundaries in the uneven layer. The stability of η maintained to be about 8% over 28 days.

In addition of 10% FAI and 1% or 2% $EuBr_2$, the photovoltaic performances of J_{SC}, FF, R_{sh} and EQE were reduced, yielding η of 4.85% and 4.67%. Addition of FAI and $EuBr_2$ reduced the stability of η during 30 days. The Br anions were distributed at grain boundaries, and was not efficiently inserted into defects in the perovskite crystal owing to difficulty in Br anion diffusion in the perovskite layer. In the standard case using 20% FAI, the photovoltaic parameters of J_{SC}, V_{oc}, R_s, R_{sh} and EQE were improved, yielding η of 8.13%. The stability was gradually reduced.

In the additive case of 20% FAI, 2% $Tb(acac)_3$ or $Sm(acac)_3$ under the annealing treatment, the photovoltaic performance of J_{SC}, V_{oc}, FF, R_{sh} and EQE were improved, yielding increase of η to be 7.93% and 4.79% for $Tb(acac)_3$ and $Sm(acac)_3$ system. The strengths of EQE significantly increased in the range of 400-800 nm. The annealing treatment optimized with tuning the internal structure while promoting the crystal generation and growth. The electric current was efficiently converted from the photon, increasing J_{SC} and EQE. However, the stabilities of η were drastically reduced to be less than 1% in 1 week. The acetylacetonate hydrate with steric hindrance did not diffuse and introduce into ligands, yielding no-passivation.

The photovoltaic properties of J_{SC}, R_s and η of the Eu^{3+}, Sm^{2+} or Tb^{3+}-doped perovskite crystals were analyzed by the electronic structures [30]. The electron density distribution, band structures, and PDOS of Eu^{2+}, Sm^{2+} or Tb^{3+}-doped $FAPbI_3$ crystals were discussed. As shown in Fig. 1 (a), incorporation of Eu^{2+} ion into the perovskite crystal caused the narrow band dispersion along Γ direction with effective mass ratio of electron and hole to free electron ($m_e^*/m_0 = 0.03$ and $m_h^*/m_0 = 0.01$) near CB and VB states. This behavior expects increase of the carrier mobility related to J_{sc}. The calculated band gap (E_g = 1.53 eV) was closed to the experimental results (E_g = 1.50 eV) by EQE. The PDOS showed narrow dispersion of 3d orbital, the separated 4f orbital of Eu atom, 5p orbital of I atom near VB state, and 6p orbital of Pb atom and d orbital of Eu atom near CB state. The charge transfer between 3d-5p orbital in Eu and I atom, 3d-6p orbital in Eu and Pb atom caused the carrier generation and diffusion, yielding increase of J_{sc}.

The electron density distribution, band structures, PDOS of Sm^{2+}-doped $FAPbI_3$ crystal were calculated. As shown in Fig. 1 (b), the 3d and 5d orbital of Sm ion were localized near VB and CB states. The theoretical band gap (E_g = 0.4 eV) was fairly narrowed, as compared with the experimental band gap (E_g = 1.57 eV) by EQE. The narrow band gap of d orbital of Sm ion was derived from the slight distortion between the Sm-I bonds as Jahn-Teller effect. The flat band distribution near VB state indicates the suppression of the hole-diffusion, expecting decrease of J_{SC}.

The electron density distribution, band structures, and PDOS of Tb^{3+}-doped $FAPbI_3$ crystal were calculated. As shown in Fig. 1 (c), the 4f orbital of Tb atom was localized near VB state. The d orbital of Tb atom and 6p orbital of Pb atom stated near CB state. The 4f orbital of Tb atom was localized, and 5p orbital of I atom stated near VB state. The calculated direct band gap of 1.49 eV was closed to the experimental band gap (E_g = 1.59 eV) converted by EQE. The flat band dispersion consisting with the localized 4f orbital of Tb atom near VB state expects as inhibiting the hole-diffusion, decreasing J_{SC} related to η.

The photovoltaic behavior were analyzed on the basis of the electron structures. Especially, partial replacement of Eu^{2+} ion with B-site of Pb atom caused the narrow band dispersion with decrease of the effective mass, promoting the carrier diffusion related to J_{sc}. The Eu^{2+} cation and Cl^- anion were distributed at grain boundaries, and were efficiently inserted into defects on lead or halogen site in the crystal as passivation effect. The Eu-doped perovskite crystal was nucleated and reformed by the Eu^{2+} / Eu^{+3} redox reaction.

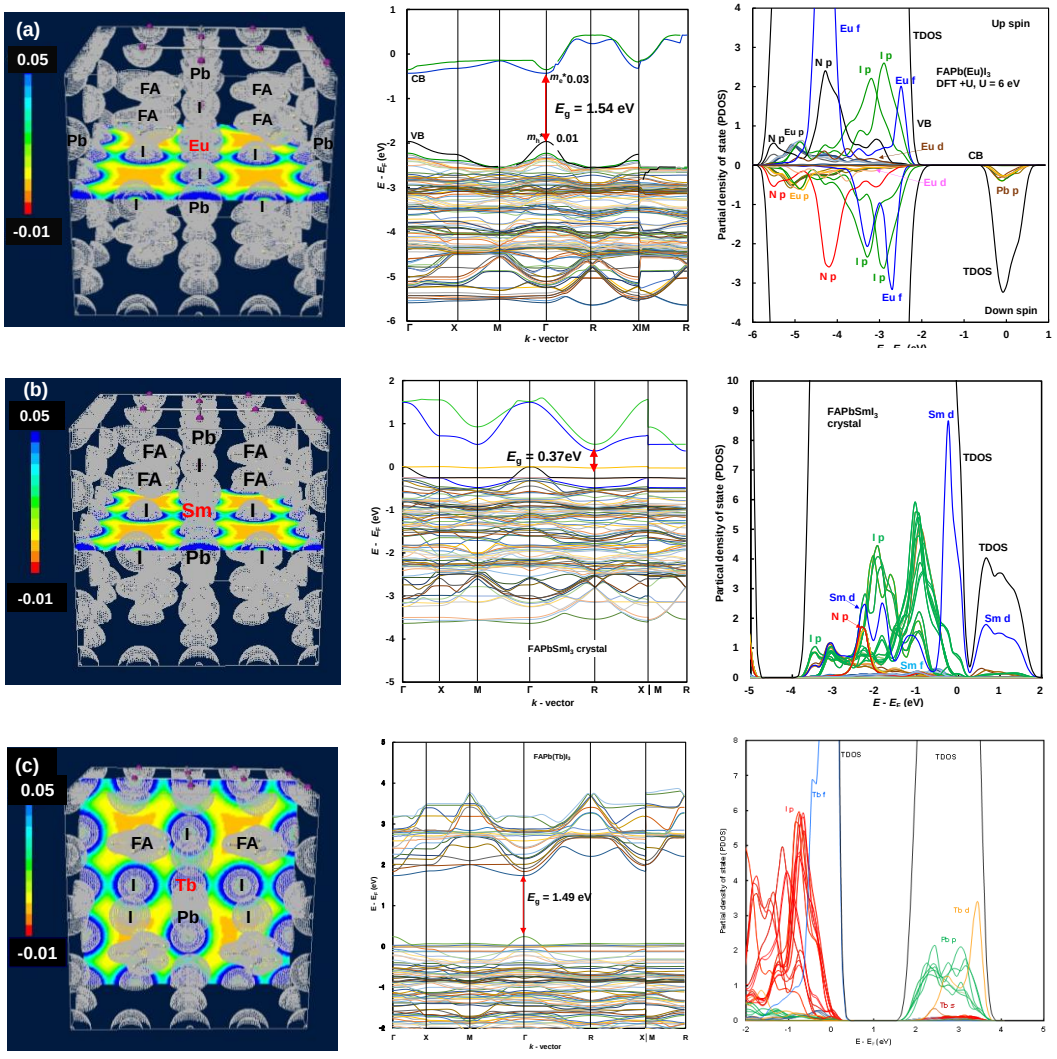

Fig. 1. Electronic density distribution, band structures, partial and total density of states (PDOS) of (a) Eu^{2+}-, (b) Sm^{2+}- and (c) Tb^{3+}-doped $FAPbI_3$ perovskite crystals.

Incorporation of Sm^{2+} or Tb^{3+} ion into the crystal reduced the performance as the decomposition owing to no-redox reaction. The photovoltaic performance was based on the flat band dispersion of the localized 4f orbital of Sm^{2+} ion and d orbital of Tb^{3+} ion near VB state. The acetylacetonate hydrate anion were not inserted into defects at halogen site in the crystal, suggesting a loss of passivation effect. The organic anions with steric hindrance were difficult to diffuse and located as ligands in the crystal. The Sm^{2+}- or Tb^{3+}-doped perovskite crystal were gradually decomposed by desorption of MA and I ions. The Eu-doped perovskite crystal have advantage to apply for the industrial photovoltaic devices with long-term stability of conversion efficiency. The lanthanide-doped perovskite crystal had the photovoltaic characteristics based on the electronic structure, kinetics and thermodynamic behavior of cation and anion in the perovskite crystal.

5. Conclusions

Fabrication and characterization of the lanthanide compound doped perovskite solar cells were performed for improving the photovoltaic performance with stability of conversion efficiency. Incorporation of FAI and $EuCl_2$, $EuBr_2$, $Sm(acac)_3$ or $Tb(acac)_3$ into the perovskite crystals on the photovoltaic performance were investigated. The addition of

FAI and $EuCl_2$ improved the photovoltaic performance of J_{SC}, EQE and η. The photovoltaic properties were based on the narrow band dispersion with decrease of effective mass. The carrier mobility related to Jsc depends on the charge transfer between 3d orbital of Eu atom, 5p orbital of iodine atom and 6p orbital of Pb atom in the crystal. Addition of $Sm(acac)_3$ or $Tb(acac)_3$ reduced the photovoltaic performances of J_{SC}, EQE and the stability of η. The behavior was due to the flat band dispersion of the d orbital of Sm^{2+} ion and 4f orbital of Tb^{3+} ion near VB state. The stability was not maintained due to the absence of redox reaction based on charge transfer. The lanthanide-doped perovskite crystal had the photovoltaic characteristics based on the electronic structure. The Eu-doped perovskite crystal have advantage to apply for the photovoltaic devices with stability.

Author Contributions: All authors contributed to the study conception and design. Material preparation, characterization, data collection and analysis were performed by A.S., K.K., T.O., M.O., S.F. and T.T. The first draft of the manuscript was written by A.S. and all authors commented on previous versions of the manuscript. All authors read and approved the final manuscript.

Funding: This work was supported by JSPS KAKENHI Grant Number JP 21K05261.

Data Availability Statement: Not applicable. All data generated and analyzed during this study are included in this published article.

Conflicts of Interest: The authors declare no conflict of interest.

References

1. Jeong, M.; Choi, I.W.; Go E. M.; Cho, Y.; Kim, M.; Lee, B.; Jeong, S.; Jo, Y.; Choi; H.W.; Lee J.; Bae, J.H.; Kwak, S.K.; Kim, D.S.; Yang, C.; Stable perovskite solar cells with efficiency exceeding 24.8% and 0.3-V voltage loss, *Science* **2020**, *369*, 1615-1620.
2. Jeong, J.; Kim, M.; Seo, J.; Lu, H.; Ahlawat, P.; Mishra, A.; Yang, Y.; Hope, M.A.; Eickemeyer, F.T.; Kim, M.; Yoon, Y.J.; Choi, I.W.; Darwich, B.P.; Choi, S.J.; Jo, Y.; Lee, J.H., Walker B.; Zakeeruddin S.M.; Emsley, L.; Rothlisberger, U.; Hagfeldt, A.; Kim, D.S.; Grätzel, M.; Kim, J.Y.; Pseudo-halide anion engineering for α-$FAPbI_3$ perovskite solar cells, *Nature* **2021**, *592*, 381-385.
3. Dai, Z.; Yadavalli, S.K.; Chen, M.; Abbaspourtamijani, A.; Qi, Y.; Padture, N.P.; Interfacial toughening with self-assembled monolayers enhances perovskite solar cell reliability, *Science*, **2021**, *372*, 618-622.
4. Tanga, Z.; Uchida, S.; Bessho, T.; Kinoshita, T.; Wang, H.; Awai, F.; Jono, R.; Maitani, M.M.; Nakazaki, J.; Kubo, T.; Segawa, H.; Modulations of various alkali metal cations on organometal halide perovskites and their influence on photovoltaic performance, *Nano Energy*, **2018**, *45*, 184-192.
5. Chen, Y.; Li, N.; Wang, L.; Li, L.; Xu, Z.; Jiao, H.; Liu, P.; Zhu, C.; Zai, H.; Sun, M.; Zou, W.; Zhang, S.; Xing, G.; Liu, X.; Wang, J.; Li, D.; Huang, B.; Chen, Q.; Zhou, H.; Impacts of alkaline on the defects property and crystallization kinetics in perovskite solar cells, *Nat. Commun.* **2019**, *10*, 1112.
6. Oku, T.; Kandori, S.; Taguchi, M.; Suzuki, A.; Okita, M.; Minami, S.; Fukunishi, S.; Tachikawa, T.; Polysilane-inserted methylammonium lead iodide perovskite solar cells doped with formamidinium and potassium, *Energies*, **2020**, *13*, 4776.
7. Song, S.; Yang, S.J.; Choi, W.; Lee, H.; Sung, W.; Park, C.; Ch, K.; Molecular engineering of organic spacer cations for efficient and stable formamidinium perovskite solar cell, *Adv. Energy. Mater.* **2020**, *10*, 2001759.
8. Jodlowski, A.D.; Carmona C.R.; Grancini, G.; Salado, M.; Ralaiarisoa, M.; Ahmad, S.; Koch, N.; Camacho, L.; Miguel, G.; Nazeeruddin, M.K.; Large guanidinium cation mixed with methylammonium in lead iodide perovskites for 19% efficient solar cells, Nat. *Energy*, **2017**, *2*, 972-979.
9. Kishimoto, T.; Oku, T.; Suzuki, A.; Ueoka, N.; Additive effects of guanidinium iodide on $CH_3NH_3PbI_3$ perovskite solar cells, *Phys. Status Solidi A* **2021**, *218*, 2100396.
10. Gao, L.;, Li, X.; Liu, Y.; Fang, J.; Huang, S.; Spanopoulos, I.; Li, X.; Wang, Y.; Chen, L.; Yang, G.; Kanatzidis, M.G.; Incorporated guanidinium expands the $CH_3NH_3PbI_3$ lattice and enhances photovoltaic performance, *ACS Appl. Mater. Interfaces* **2020**, *12*, 43885-43891.
11. Nishi, K.; Oku, T.; Kishimoto, T.; Ueoka, N.; Suzuki, A.; Photovoltaic characteristics of $CH_3NH_3PbI_3$ perovskite solar cells added with ethylammonium bromide and formamidinium iodide, *Coatings*, **2020**, *10*, 410.
12. Peng, L.; Xie, W.; Theoretical and experimental investigations on the bulk photovoltaic effect in lead-free perovskites $MASnI_3$ and $FASnI_3$, *RSC Advances* **2020**, *10*, 14679-14688.
13. Suzuki, A.; Oku, T.; Effects of transition metals incorporated into perovskite crystals on the electronic structures and magnetic properties by first principles calculation, *Heliyon* **2018**, *4*, e00755.
14. Ueoka, N.; Oku, T.; Suzuki, A.; Additive effects of alkali metals on Cu-modified $CH_3NH_3PbI_{3-\delta}Cl_\delta$ photovoltaic devices, *RSC Adv.* **2019**, *9*, 24231.
15. Ueoka, N.; Oku, T.; Effects of co-addition of sodium chloride and copper (II) bromide to mixed-cation mixed-halide perovskite photovoltaic devices, *ACS Appl. Energy Mater.* **2020**, *3*, 7272-7283.

16. Suzuki, A.; Oe, M.; Oku, T.; Fabrication and characterization of Ni-, Co-, and Rb-incorporated $CH_3NH_3PbI_3$ perovskite solar cells, *J. Electron. Mater.* **2021**, *50*, 1980-1995.
17. Wang, L.; Zhou, H.; Hu, J.; Huang, B.; Sun, M.; Dong, B.; Zheng, G.; Huang, Y.; Chen, Y.; Li, L.; Xu, Z.; Li, N.; Liu, Z.; Chen, Q.; Sun, L.D.; Yan, C.H.; A Eu^{3+}-Eu^{2+} ion redox shuttle imparts operational durability to Pb-I perovskite solar cells, *Science,* **2019**, *363*, 265-270.
18. Suzuki, A.; Oku, T.; Effects of mixed-valence states of Eu-doped $FAPbI_3$ perovskite crystals studied by first-principles calculation, *Mater. Adv.* **2021**, *2*, 2609-2616.
19. Liu, S.; Guan, Y.; Sheng, Y.; Hu, Y.; Rong, Y.; Mei, A.; Han, H.; A review on additives for halide perovskite solar cells, *Adv. Energy Mater.* **2019**, *10*, 1902492.
20. Oku, T.; Crystal structures of perovskite halide compounds used for solar cells, *Rev. Adv. Mater. Sci.* **2020**, *59*, 264-305.
21. Suzuki, A.; Oku, T.; First-principles calculation study of electronic structures of alkali metals (Li, K, Na and Rb)-incorporated formamidinium lead halide perovskite compounds, *Appl. Surf. Sci.* **2019**, *483*, 912-921.
22. Suzuki, A.; Miyamoto, Y.; Oku, T.; Electronic structures, spectroscopic properties, and thermodynamic characterization of sodium- or potassium-incorporated $CH_3NH_3PbI_3$ by first-principles calculation, *J. Mater. Sci.* **2020**, *55*, 9728-9738.
23. Suzuki, A.; Oku, T.; Electronic structures and magnetic properties of transition metal doped $CsPbI_3$ perovskite compounds by first-principles calculation, *Phys. Solid State,* **2019**, *61*, 1074-1085.
24. Song, Z.; Xu, W.; Wu, Y.; Liu, S.; Bi, W.; Chen, X.; Song, H.; Incorporating of lanthanides ions into perovskite film for efficient and stable perovskite solar cells, *Small*, **2020**, *16*, 2001770.
25. Chen, L.; Wu, W.; Wang, J.; Qian, Z.; Liu, R.; Niu, Y.; Chen, Y.; Xie, X.; Zhang, H.; Lanthanide stabilized all-inorganic $CsPbI_2Br$ perovskite solar cells with superior thermal resistance, *ACS Appl. Energy Mater.* **2021**, *4*, 3937-3944.
26. Chen, Y.; Liu, S.; Zhou, N.; Li, N.; Zhou, H.; Sun, L.D.; Yan, C.H.; An overview of rare earth coupled lead halide perovskite and its application in photovoltaics and light emitting devices, *Prog. Mater. Sci.* **2021**, *120*, 100737.
27. Karunakaran, S.K.; Arumugam, G.M.; Yang, W.; Ge, S.; Khan, S.N.; Lin, X.; Yang, G.; Research progress on the application of lanthanide-ion-doped phosphor materials in perovskite solar cells, *ACS Sustainable Chem. Eng.* **2021**, *9,* 1035–1060.
28. Suzuki, A.; Kishimoto, K.; Oku, T.; Okita, M.; Fukunishi, S.; Tachikawa, T.; Additive effect of lanthanide compounds into perovskite layer on photovoltaic properties and electronic structures, *Synthetic Metals* **2022**, *287,* 117092.
29. Taguchi, M.; Suzuki, A.; Oku, T.; Ueoka N.; Minami, S.; Okita, M.; Effects of annealing temperature on decaphenylcyclopentasilane-inserted $CH_3NH_3PbI_3$ perovskite solar cells, *Chem. Phys. Lett.* **2019**, *737*, 136822-1–7.
30. Oku, T.; Taguchi, M.; Suzuki, A.; Kitagawa, K.; Asakawa, Y.; Yoshida, S.; Okita, M.; Minami, S.; Fukunishi, S.; Tachikawa, T.; Effects of polysilane addition to chlorobenzene and high temperature annealing on $CH_3NH_3PbI_3$ perovskite photovoltaic devices, *Coatings* **2021**, *11*, 665.
31. Uvarov, V.; Popov, I.; Metrological characterization of X-ray diffraction methods for determination of crystallite size in nanoscale materials, *Mater. Charac.* **2013**, *85*, 111.
32. Mashiyama, H.; Kurihara, Y.; Azetsu, T.; Disordered cubic perovskite structure of $CH_3NH_3PbX_3$ (X = Cl, Br, I), *J. Korean Phys. Soc.* **1998**, *32,* S156-S158.
33. Oku, T.; Solar cells and energy materials. De Gruyter, Berlin. **2017**.